Research Square

Preprints are preliminary reports that have not undergone peer review.
They should not be considered conclusive, used to inform clinical practice,
or referenced by the media as validated information.

Clinical utility of age-matched z-score maps from a large normative pediatric [^{18}F]-FDG PET database for localizing epileptogenic abnormalities: illustrative cases

Seokbeen Lim
Mayo Clinic https://orcid.org/0000-0002-4142-3478
Paul H. Min
Mayo Clinic
Nur Dizdar
Mayo Clinic
Miguel D. Diaz
Mayo Clinic
Julie B. Guerin
Mayo Clinic
Michelle Silvera
Mayo Clinic
Lily C. Wong-Kisiel
Mayo Clinic
Hojjat Salehinejad
Mayo Clinic
Gokce Belge Bilgin
Mayo Clinic
Cem Bilgin
Mayo Clinic
Benjamin H. Brinkmann
Mayo Clinic
Jeffrey W. Britton
Mayo Clinic
Derek R. Johnson
Mayo Clinic
Steven Messina
Mayo Clinic
Bradley J. Kemp
Mayo Clinic

A. Tuba Kendi
Mayo Clinic
Jun Zhang
Mayo Clinic
Val J. Lowe
Mayo Clinic
Brian J. Burkett
Burkett.Brian@mayo.edu

Mayo Clinic

Research Article

Keywords: Pediatric normative [18F]-FDG PET dataset, Large pediatric normative [18F]-FDG PET data cohort, Epilepsy, Age-matched z-score analysis, Quantitative localization of epileptogenic abnormalities

Posted Date: September 24th, 2026

DOI: https://doi.org/10.21203/rs.3.rs-11143642/v1

License: This work is licensed under a Creative Commons Attribution 4.0 International License.
Read Full License

Additional Declarations: The authors declare no competing interests.

Abstract

Introduction

Quantitative interpretation of pediatric brain [^{18}F]-FDG PET is limited by the lack of age-matched normative reference databases, despite substantial developmental variation in cerebral glucose metabolism. This study aimed to construct a large-scale normative pediatric [^{18}F]-FDG PET database and develop an age-specific z-score mapping framework for quantitative evaluation of pediatric epilepsy.

Method

Pediatric brain PET data were retrospectively derived from clinically acquired whole-body or dedicated [^{18}F]-FDG PET examinations in participants 0–19 years of age without neurologic disease or visible brain abnormalities. A total of 417 PET scans from 341 participants were stratified into five developmental age groups: infancy, early childhood, middle childhood/school age, adolescence, and late adolescence. SUVR maps were generated using whole-brain atlas and brainstem reference regions. Voxel-wise t-test analyses were performed to characterize age- and sex-related metabolic differences. Age-specific voxel-wise mean and standard deviation maps were generated from the normative cohort and used to calculate age-matched hypometabolic z-score maps in 14 pediatric patients with epilepsy. The resulting abnormalities were qualitatively evaluated for concordance with epileptogenic findings identified on clinical MRI and/or PET by expert image review.

Results

Voxel-wise analyses demonstrated prominent age-dependent SUVR differences, particularly between infancy and older age groups. With whole-brain atlas normalization, older children showed progressively higher relative SUVR in cortical and cerebellar gray matter regions, whereas infancy showed relatively higher SUVR in the occipital cortex, white matter, thalamus, and brainstem. Brainstem normalization produced distinct developmental patterns, emphasizing higher white matter SUVR in infancy and broader gray matter differences in older groups. Sex-related differences were limited and regionally specific. Whole-brain atlas normalization showed lower variability than brainstem normalization and was selected for z-score mapping. In representative epilepsy cases, age-matched z-score maps identified focal or regional hypometabolism corresponding to malformations of cortical development, focal cortical dysplasia, mesial temporal sclerosis, nonlesional MRI cases, remote insult, tumor-related abnormalities, and Sturge-Weber syndrome.

Discussion

A large-scale normative pediatric [18F]-FDG PET database can support developmentally appropriate quantitative interpretation of pediatric brain PET. Age-matched z-score mapping may complement visual assessment by highlighting abnormal cerebral glucose metabolism in pediatric epilepsy, although findings should be interpreted with MRI, EEG, seizure semiology, and other presurgical data.

Introduction

Pediatric epilepsy is the most common chronic neurologic disorder in childhood, and its epidemiologic burden varies across developmental stages [1, 2]. Incidence rates are highest during the first year of life and again between 5 and 9 years of age [1, 2]. In North America and Europe, the incidence of epilepsy during infancy, defined as younger than 1 year of age, has been reported to range from 90 to 212 per 100,000 population, whereas the global prevalence of epilepsy in children 5 to 9 years of age is reported to be 374.9 per 100,000 population [1, 2]. Neurodevelopmental and behavioral comorbidities associated with pediatric epilepsy can substantially worsen the quality of life in affected children [3]. In addition, the developing brain is particularly vulnerable to cognitive and neurobehavioral comorbidities when exposed to persistent seizures and ongoing epileptiform activity [3]. Cognitive and neurobehavioral comorbidities are common in the setting of pediatric epilepsy and include intellectual disability of varying severity, specific learning disorders, autism spectrum disorder, and attention deficit hyperactivity disorder, particularly the predominantly inattentive presentation [3]. In a population-based study of school-aged children with epilepsy, 80% of those with active epilepsy exhibited either a behavioral disorder or cognitive impairment [4]. Antiepileptic drugs (AEDs) are the first-line treatment for patients with epilepsy, and most patients with seizure symptoms achieve adequate seizure control with pharmacologic therapy [5, 6]. However, approximately 20% or more develop drug-resistant epilepsy, in which seizures remain uncontrolled despite appropriate AED treatment [7-9]. In these patients, surgical resection or other destructive procedures of the epileptogenic zone can result in excellent outcomes for seizure control, but surgical success is critically dependent on accurate localization of the epileptogenic focus [9].

Neuroimaging modalities play a critical role in localizing the epileptogenic focus, guiding surgical planning to maximize seizure control while preserving eloquent cortex [6, 8]. Among these modalities, [^{18}F]-FDG PET can localize abnormalities in epilepsy by depicting cerebral glucose metabolism with uptake of FDG, a glucose analog transported into brain tissue through glucose transporters [6, 10, 11]. In epilepsy, [^{18}F]-FDG PET enables both visualization and quantification of regional cerebral hypometabolism. Focal glucose hypometabolism during the interictal or postictal period can indicate the location of an epileptogenic lesion or functionally abnormal cortex in the epileptogenic zone, even some patients with normal MRI [6]. Kumar et al. evaluated focal hypometabolism on [^{18}F]-FDG PET in pediatric patients with intractable focal epilepsy using both visual interpretation and voxel-based statistical parametric mapping (SPM) analysis [12]. Voxel-based analysis achieved accurate lesion lateralization in 100% of cases, compared with 90% for visual interpretation, and identified 7 of 9 seizure-onset zones that were missed on visual review [12]. These findings support the value of objective quantitative PET analysis as a complementary tool for preoperative localization of epileptogenic abnormalities [12]. To evaluate metabolic alterations associated with epileptogenic abnormalities, the asymmetry index has been used as a quantitative measure of interhemispheric differences in glucose metabolism on [^{18}F]-FDG PET [5, 13, 14]. In a longitudinal [^{18}F]-FDG PET study of pediatric epilepsy, Hu et al. showed that patients with drug-resistant epilepsy exhibited significantly greater metabolic asymmetry than those with drug-responsive epilepsy at both baseline and follow-up [5]. The drug-resistant group also demonstrated more extensive and progressive metabolic decline, accompanied by less efficient brain network organization [5]. In addition, Z-score–based parametric analysis has been investigated as an objective

approach for localizing epileptogenic abnormalities on [^{18}F]-FDG PET. Using CortexID Suite, Li et al. showed that quantitative z-score analysis provided diagnostic performance comparable to visual interpretation. Combined visual and quantitative assessment further improved localization, yielding AUC values of 0.971 for medial temporal lobe epilepsy and 0.897 for lateral temporal lobe epilepsy [15].

Despite substantial progress in objective approaches for evaluating epileptogenic lesions or functional abnormalities with [^{18}F]-FDG PET, continued efforts are needed to refine quantitative methods for characterizing PET-defined lesions and abnormalities and to optimize their translation into clinical practice. Statistical parametric mapping, such as z-score parametric, provides a valuable objective framework for localizing epileptogenic abnormalities on brain [^{18}F]-FDG PET [15]. However, no widely available clinical tool currently enables individual pediatric brain [^{18}F]-FDG PET scans to be interpreted against an age-matched normative pediatric database. Existing commercial platforms primarily rely on adult reference databases and are generally designed to support the evaluation of neurodegenerative disorders [15]. Application of older adult normative data to quantification of pediatric brain FDG PET is presumably an inaccurate representation because cerebral glucose metabolism is known to be age-dependent in infants and children [16, 17]. Although recent efforts have sought to develop pediatric normative databases, the construction of large-scale reference datasets remains challenging because of ethical and practical limitations in prospectively acquiring PET data from healthy children [18]. A previous study that retrospectively collected brain PET scans from neurologically normal pediatric patients has demonstrated the feasibility of establishing pediatric-specific large normative databases for clinical PET interpretation [19]. To our knowledge, no previous literature has described the use of a pediatric database to generate age-specific FDG PET quantitative maps as an interpretive aid for pediatric epilepsy. Accordingly, the present study aimed to construct a large-scale normative pediatric brain [^{18}F]-FDG PET database and develop an age-matched z-score mapping framework for quantitative image interpretation. We further evaluated, through illustrative pediatric epilepsy cases, whether this database-driven approach could facilitate the detection and localization of epileptogenic hypometabolism and other abnormal FDG uptake patterns, supporting its potential development as a quantitative clinical tool.

Materials and Methods

2.1 Participants

In this study, brain PET data were derived from whole body [^{18}F]-FDG PET examinations performed at Mayo Clinic for the clinical evaluation of non-neurologic conditions, including oncologic indications. We retrospectively identified PET scans from pediatric participants 19 years of age or younger in whom the entire brain was included within the imaging field of view. PET scans were excluded if visual review demonstrated structural or metabolic brain abnormalities, if image quality was insufficient for analysis, or if electronic medical record review indicated a history of neurologic disease at the time of imaging. Using these criteria, 341 participants were included in the study as a large normative dataset. The cohort

comprised 198 male and 143 female participants, with mean ages of 11.04 ± 6.43 years and 12.05 ± 6.17 years, respectively (p=0.11). Because some participants underwent PET imaging more than once, longitudinal handling procedures were applied. When multiple scans were acquired within the same age range, those images were averaged so that each participant contributed a single representative image to that age stratum. When repeated scans were acquired across different age ranges, the images were retained separately so that each scan contributed to the age-appropriate normative group. After incorporating these repeated measurements according to age range assignment, the final dataset consisted of 417 pediatric [^{18}F]-FDG PET scans, which are summarized in table 1. Participants were stratified into five study-defined age groups based on developmentally informed pediatric age categories: infancy (0–1 years), early childhood period (2–5 years), middle childhood/school age (6–12 years), adolescence (13–17 years), and late adolescence (18–19 years) to be used age-matched z-score analysis.

A total of 14 patients with epilepsy were included in this study. For each patient, an epileptogenic lesion was identified on MRI and/or PET was confirmed on review of cross-sectional images by a board-certified nuclear radiologist and neuroradiologist with 4 years of experience. The corresponding imaging findings are summarized in table 2.

The retrospective study was reviewed and determined to be exempt by the Mayo Clinic Rochester Institutional Review Board.

2.2 Imaging processing

Participants received an intravenous [^{18}F]-FDG weight-based dose of 3.7-5.18 MBq x patient weight (kg) for whole body PET and 3.7 MBq x patient weight (kg) for dedicated brain PET, with a minimum dose of 37 MBq, approximately 60 minutes prior to scanning using a standardized image acquisition protocols. The body PET acquisition took 3 minutes per bed position and for those with epilepsy, the dedicated brain PET acquisition took 10 minutes.

The collected whole-body PET scans were manually cropped to isolate the brain using commercially available MIMneuro software (MIM Software Inc., USA), as shown in the Figure S1. Subsequent image preprocessing was performed in AFNI software [20, 21]. Each cropped PET volume was resampled and spatially normalized to the MNI152 PET template [22] grid using *3dresample* and *3dAllineate*. Voxel-wise SUVR images were then generated using brainstem and whole brain reference regions defined on the MNI152 template atlas [23, 24] separately, with normalization performed using *3dcalc* and *3dmaskave*. The resulting preprocessed voxel-wise SUVR volumes were stratified according to five age groups and sex and were then used for downstream analyses.

2.3 Age-matched z-score map calculation

Participants were stratified into five study-defined age groups based on developmentally informed pediatric age categories, as listed in the participant section. After assignment of normative individual voxel-wise SUVR images to their corresponding age-defined groups, group-level mean and standard deviation images were generated for each stratum. These age-specific normative maps were subsequently used to compute voxel-wise z-score maps for the preprocessed brain PET scans of epilepsy patients, matched to the appropriate age group as follows.

$$z = \frac{X - \mu}{\sigma}$$

In this equation, z denotes the voxel-wise z score, X represents the SUVR value at each voxel, μ denotes the mean voxel-wise SUVR, and σ denotes the corresponding voxel-wise standard deviation. The resulting z-score map was thresholded at 1.96, corresponding to a p-value of 0.05, to retain only statistically significant voxels. Because the analysis was specifically designed to detect hypometabolic abnormalities, only voxels in the negative direction of the distribution were preserved, rather than applying a two-sided threshold. Both the z-score maps and the thresholded z-score maps were transformed from template space back to individual subject space and visualized in both template and individual spaces for the illustrative case analyses.

2.4 Statistical analysis

Voxel-wise group comparison analyses were performed to characterize differences across the five age groups. Group-level statistical testing was conducted using AFNI *3dttest++*. The resulting statistical maps were thresholded and visualized using a multiple comparison corrected significance threshold of q = 0.05. In addition, voxel-wise group comparison analysis was performed using the same approach to evaluate sex related differences between male and female participants, and these results were likewise visualized at a corrected threshold of q = 0.05.

Results

3.1 Normative [^{18}F]-FDG PET voxel-wise analysis

Figure 1 presents voxel-wise t-test comparisons of SUVR across the five pediatric age groups. Voxel-wise SUVR maps normalized to the whole-brain atlas reference region were used for this analysis. Red voxels denote regions with higher SUVR in group B than in group A, whereas blue voxels denote regions with higher SUVR in group A than in group B. Compared with the infancy group (0–1 year), older age groups showed progressively greater differences in cortical gray matter metabolism, particularly in the frontal, temporoparietal, and cerebellum regions. Conversely, compared with the four older age groups, the infancy group demonstrated relatively higher SUVR in the occipital cortex, white matter, thalamus, and brainstem. When the early childhood group (2–5 years) was compared with the middle

childhood/school-age group (6–12 years), higher SUVR in the middle childhood/school-age group was observed in localized voxels within regions of the cerebellar gray matter, temporal cortex, insula cortex, anterior cingulate cortex and frontal pars opercularis. By contrast, the early childhood group showed relatively higher SUVR in the occipital and parietal lobes. In comparisons involving adolescence (13–17 years) and late adolescence (18–19 years), these differences became more spatially widespread and increased in magnitude. In comparisons with the early childhood group, both the adolescence and late adolescence groups exhibited more prominent SUVR differences across deep brain structures, including the brainstem and thalamus, and temporal lobe–associated regions, including the hippocampus, entorhinal cortex, amygdala, and parahippocampal gyrus. Compared with the middle childhood/school-age group (6–12 years), both the adolescence (13–17 years) and late adolescence (18–19 years) groups demonstrated higher SUVR in temporal lobe–associated structures, including the hippocampus, entorhinal cortex, amygdala, and parahippocampal gyrus. Additional differences were observed in the anterior cingulate cortex, insula, and transverse temporal cortex. Conversely, the middle childhood/school-age group exhibited higher metabolism in the occipital and parietal lobes and broadly distributed white matter regions. No significant group differences were found between adolescence and late adolescence.

When SUVR was calculated using the brainstem as the reference region, voxel-wise group comparisons revealed age-related patterns that differed from those obtained using the whole-brain atlas reference region (Figure S2). Compared with the infancy group (0–1 year), the early childhood group exhibited higher SUVR throughout widespread gray matter regions. The middle childhood/school-age group showed more prominent SUVR differences in the frontal, temporal, and parietal cortices, as well as in cerebellar gray matter. By contrast, the infancy group demonstrated relatively higher SUVR in white matter regions. This white matter–dominant pattern in infancy became more apparent in comparisons with the adolescence and late adolescence groups, whereas occipital lobe differences were progressively attenuated. Compared with the early childhood group, the middle childhood/school-age group showed higher localized SUVR in the temporal cortex, precentral and postcentral cortices, and cerebellar gray matter, whereas the early childhood group showed higher SUVR in white matter and occipital regions. Unlike the voxel-wise t-test findings using the whole brain atlas reference region, comparisons with the adolescence and late adolescence groups showed higher SUVR in the older groups only in localized voxels within selected regions, including the superior frontal cortex, temporal cortex, insula, cerebellar gray matter, and brainstem. Overall, however, the early childhood group showed higher SUVR across broader brain regions. A similar pattern was observed when the middle childhood/school-age group was compared with the adolescence and late adolescence groups, with higher overall SUVR in the middle childhood/school-age group except in localized voxels within superior frontal and deep brain regions. No significant differences were found between the adolescence and late adolescence groups.

Voxel-wise t-test analyses were additionally conducted to evaluate sex-related SUVR differences using both whole-brain and brainstem reference regions (Figure S3). The overall spatial patterns were similar between the two reference methods. With whole-brain normalization, females showed higher SUVR than

males in the localized voxels within temporal cortical regions, including the fusiform and middle temporal cortices, as well as in the precentral, postcentral, insular, anterior cingulate, lingual, and parietal cortices. In contrast, males showed higher SUVR in localized voxels within orbitofrontal, cerebellar gray matter, and lateral ventricular regions. Brainstem-normalized analyses demonstrated a comparable pattern.

3.2 Age-stratified normative FDG-PET templates for z-score map generation

For patient-level z-score calculation, age-specific normative mean and standard deviation maps were generated from the pediatric [^{18}F]-FDG PET reference cohort. Whole-brain atlas–normalized mean SUVR maps demonstrated relatively consistent spatial patterns across the five age groups (Figure S4). However, the corresponding standard deviation maps revealed age-specific variability, with the early childhood group showing the highest variance in the occipital lobe (Figure S4).

When the brainstem was used as the reference region, mean SUVR maps again showed broadly similar spatial distributions across age groups but had higher overall SUVR values than those generated with whole-brain atlas normalization (Figure S5). Among the five age groups, the early childhood and middle childhood/school-age groups demonstrated the highest mean SUVR values (Figure S5). Brainstem-normalized standard deviation maps also demonstrated greater variance than whole-brain atlas–normalized maps, with prominent occipital variance in the infancy, early childhood, and middle childhood/school-age groups (Figure S5). The middle childhood/school-age group additionally showed increased variance in the frontal and temporal cortices (Figure S5).

For patient-level z-score mapping, we used age-specific mean and standard deviation maps generated from SUVR images normalized to the whole-brain atlas reference region, as this approach demonstrated lower variability than brainstem normalization.

3.3 Case-based age-specific z-score analysis in malformations of cortical development and focal cortical dysplasia

We grouped cases with focal cortical dysplasia (FCD), polymicrogyria, and related cortical abnormalities under the category of malformations of cortical development/focal cortical dysplasia listed in the clinical diagnosis from Table 2. Malformations of cortical development have characteristic MRI features such as cortical thickening, abnormal gyration, or gray-white matter blurring, which may be accompanied by localized hypometabolism on interictal FDG-PET. Therefore, this diagnostic category was used to demonstrate the ability of age-matched z-score mapping to highlight epileptogenic cortical abnormalities, including lesions that may be subtle and difficult to detect on structural MRI.

Participant #1 was 1 year old at imaging and had focal cortical dysplasia in the left precentral gyrus (Figure 2A). Z-score maps generated in both MNI template and individual MRI spaces showed localized negative z-scores in the left precentral cortex, corresponding to the arrow-indicated region. The corresponding SUVR map demonstrated reduced uptake, consistent with focal hypometabolism.

Participant #2 was 1 year old at imaging and had focal cortical dysplasia in the left frontal gyrus (Figure 2B). In both MNI template and individual MRI spaces, z-score maps showed localized negative z-scores in the left rostral middle frontal cortex, corresponding to the arrow-indicated region. The SUVR map demonstrated reduced uptake in the same region, consistent with focal hypometabolism.

Participant #3 was 8 years old at imaging and showed abnormalities consistent with focal cortical dysplasia involving the right Sylvian fissure/superior temporal gyrus (Figure 2C). Z-score maps generated in both MNI template and individual MRI spaces demonstrated extensive negative z-score abnormalities in the corresponding right Sylvian fissure/superior temporal region. The SUVR map showed reduced uptake in the same area, consistent with focal hypometabolism.

Participant #7 was 12 years old at imaging and had findings of a focal cortical dysplasia in the left gyrus rectus (Figure 2D). In both MNI template and individual MRI spaces, z-score maps demonstrated localized negative z-scores in the left gyrus rectus, with additional broader negative z-score abnormalities in the left temporal region. Corresponding SUVR reductions were observed in these regions, consistent with hypometabolism.

Participant #9 was 14 years old at imaging and had polymicrogyria (Figure 2E). Z-score analysis in individual MRI space showed widespread negative z-score abnormalities across the right temporal, parietal, and occipital lobes, corresponding to the arrow-indicated regions. These areas showed reduced SUVR, consistent with extensive hypometabolism in the region of the malformation of cortical development.

Participant #10 was 14 years old at imaging and had findings of focal cortical dysplasia (Figure S6A). Individual-space z-score mapping showed localized negative z-scores near the temporal cortex, with corresponding SUVR reduction in the arrow-indicated region. However, localized voxels of negative z-score abnormalities were also broadly distributed across the brain. Participant #11 was 16 years old at imaging and had findings suggestive of subtle focal cortical dysplasia (Figure S6B). Individual-space z-score mapping demonstrated localized negative z-scores in the left frontal cortex, with corresponding focal SUVR reduction in the arrow-indicated region. Participant #14 was 18 years old at imaging and had findings suggestive of subtle focal cortical dysplasia (Figure S6C). Individual-space z-score mapping showed localized negative z-scores in the left Sylvian fissure/superior temporal cortex, with corresponding SUVR reduction in the arrow-indicated region. Similar to Participant 10, localized voxels of negative z-score abnormalities were also observed more diffusely across the brain.

Additional cases demonstrating subtle MRI abnormalities detected by age-matched z-score mapping are presented in Figure S7. Participant #1, previously described in Figure 2A, showed a subtle T1 MRI lesion in the left precentral gyrus consistent with suspected focal cortical dysplasia (Figure S7A). Age-matched z-score mapping demonstrated localized negative z-score abnormality at the corresponding lesion site, with additional broader negative z-score abnormalities extending across the frontal gyrus. The corresponding SUVR map showed reduced uptake in this region, consistent with hypometabolism. Participant #11, previously described in Figure S6B, showed a subtle T2 MRI lesion in the left medial

frontal cortex, suggestive of focal cortical dysplasia (Figure S7B). In contrast to Participant #1, age-matched z-score mapping in this case demonstrated a focal, well-localized negative z-score abnormality restricted to the lesion site, with corresponding focal SUVR reduction on FDG-PET, consistent with focal hypometabolism.

3.4 Case-based age-specific z-score analysis in temporal lobe epilepsy and mesial temporal sclerosis

Age-matched z-score mapping was evaluated in a representative cases of temporal lobe epilepsy with mesial temporal sclerosis, a common structural cause of epilepsy. Participant #8, a 13-year-old patient with mesial temporal sclerosis, demonstrated extensive negative z-score abnormalities across the right temporal cortex, with corresponding SUVR reduction in the arrow-indicated region (Figure 3A). These findings were consistent with right temporal hypometabolism.

3.5 Case-based age-specific z-score analysis in non-lesional MRI and structural destructive or abnormal FDG PET

Age-matched z-score mapping was evaluated in representative epilepsy cases with normal MRI exams and interictal FDG PET abnormalities. Participant #6, a 12-year-old patient with temporal lobe epilepsy and non-lesional MRI, showed extensive negative z-score abnormalities in the anterior left temporal cortex on individual-space z-score mapping (Figure 3B). The corresponding SUVR map demonstrated reduced uptake in this region, consistent with widespread temporal hypometabolism. Participant #4, a 10-year-old patient with abnormal PET findings and non-lesional MRI, showed negative z-score abnormalities in the left perirolandic region on individual-space z-score mapping (Figure 4A). The corresponding SUVR map demonstrated reduced uptake in the same region, consistent with focal hypometabolism.

3.6 Case-based age-specific z-score analysis in epilepsy associated with remote insult

Age-matched z-score mapping was evaluated in a representative cases with widespread structural abnormalities on MRI related to a remote insult. Participant #5, an 11-year-old patient with extensive right hemispheric abnormalities related to a remote insult with extensive areas of encephalomalacia, demonstrated widespread negative z-score abnormalities across the right hemisphere (Figure 4B). The corresponding SUVR map showed markedly reduced uptake, consistent with extensive right hemispheric hypometabolism.

3.7 Case-based age-specific z-score analysis in complex syndromic and tumor cases

Age-matched z-score mapping was evaluated in representative cases with structural, syndromic, or tumoral findings. Participant #12, a 17-year-old patient with a neoplasm, showed a structural abnormality on individual-space MPRAGE in the arrow-indicated region (Figure 5A). Z-score analysis demonstrated negative z-score abnormalities in the corresponding right temporal cortex, with reduced SUVR in the same region. Participant #13, a 17-year-old patient with Sturge-Weber syndrome, showed a structural abnormality on individual-space MPRAGE in the arrow-indicated region (Figure 5B) in areas of abnormal

leptomeningeal calcification characteristic of Sturg-Weber syndrome. Z-score analysis demonstrated widespread negative z-score abnormalities across the left occipital lobe, with markedly reduced SUVR in the corresponding region, consistent with extensive hypometabolism.

Discussion

The present study investigated the feasibility of constructing a large-scale normative pediatric [^{18}F]-FDG PET database and applying it to age-specific z-score mapping for quantitative evaluation of pediatric epilepsy. Developmental analyses revealed substantial age-dependent variation in SUVR patterns across childhood and adolescence, particularly between infancy and later developmental stages. With whole-brain atlas normalization, older age groups showed progressively higher relative SUVR in cortical and cerebellar gray matter regions, whereas infancy showed relatively higher SUVR in the occipital cortex, white matter, thalamus, and brainstem. These findings are consistent with the dynamic maturation of cerebral glucose metabolism during early brain development and emphasize the need for age-appropriate reference data when interpreting pediatric [^{18}F]-FDG PET [16, 25]. Reference-region selection also had a substantial effect on the observed developmental patterns. Compared with whole-brain normalization, brainstem normalization produced higher overall SUVR values and emphasized a more white matter–dominant pattern in infancy, with broader gray matter differences in older age groups. This finding suggests that quantitative pediatric [^{18}F]-FDG PET interpretation may be sensitive to the choice of normalization strategy, particularly in the developing brain where regional metabolic maturation is heterogeneous. Sex-related differences were relatively limited compared with age-related effects, although localized differences were observed in temporal, sensorimotor, insular, anterior cingulate, parietal, orbitofrontal, and cerebellar regions. Together, these findings support the importance of age-matched normative pediatric [^{18}F]-FDG PET databases and suggest that sex-informed reference models may further improve quantitative z-score interpretation in selected contexts.

As a proof-of-concept in pediatric epilepsy, the age-specific z-score maps using this large-scale normative database were applied to a variety of case-based scenarios to investigate the ability to demonstrate abnormal cerebral glucose metabolism across the broad range of imaging abnormalities that can be associated with refractory epilepsy. Clinically, the main objective of interictal [^{18}F]-FDG PET in the presurgical evaluation of refractory epilepsy is to identify potential focal abnormalities or lesions which may be targeted for surgical or destructive procedures. PET can add value in detection of these abnormalities which can be small or subtle on MRI. This was illustrated by two representative cases (Figure S7) in which age-matched z-score mapping identified regions of abnormal cerebral glucose metabolism corresponding to subtle MRI lesions that might otherwise be challenging to appreciate on visual inspection alone. Notably, the spatial extent of z-score abnormality varied between these cases—ranging from a broader distribution extending beyond the visible structural lesion to a focal abnormality tightly localized to the lesion site—suggesting that age-matched z-score mapping may capture a spectrum of metabolic derangement not always evident from structural imaging alone, and may in some instances delineate a larger region of dysfunction than is apparent on MRI. In addition, age-specific z-

score mapping identified focal regions of cerebral glucose hypometabolism in association with the selected cases, including multiple malformations of cortical development and mesial temporal sclerosis. Other structural lesions associated with pediatric epilepsy, including remote insults with encephalomalacia, tumors, and leptomeningeal calcification in Sturge-Weber Syndrome were also associated with abnormal cerebral glucose metabolism detected with age-specific z-score mapping. Interictal [^{18}F]-FDG PET can provide crucially important information in localizing epilepsy when MRI is non-lesional. Age-specific z-score mapping was able to demonstrate focal or regional cerebral glucose hypometabolism in PET scans of children with non-lesional MRI and both temporal and extratemporal epilepsy. Age-specific z-score mapping has potentially clinically utility as an aid to visual interpretation of pediatric [^{18}F]-FDG PET scans by highlighting metabolic abnormalities in these epileptogenic structural lesions.

4.1 Strengths and limitations

The normative pediatric [^{18}F]-FDG PET database developed in this study may serve as an important foundation for quantitative image analysis in pediatric epilepsy. As additional neurologically normal pediatric PET scans are incorporated, the database may become more robust and support increasingly reliable age-specific statistical mapping. By comparing individual patients with age-matched normative distributions, z-score analysis provides a developmentally appropriate framework for detecting abnormal cerebral glucose metabolism in children. This capability was particularly evident in cases with subtle structural abnormalities, where age-matched z-score mapping helped confirm and further characterize the metabolic significance of lesions that were difficult to discern on initial MRI review. Such findings underscore the potential value of this approach as a complementary tool for guiding closer radiological re-evaluation of equivocal MRI findings, particularly in the presurgical evaluation of pediatric epilepsy where subtle malformations of cortical development are common but frequently under-recognized.

Nevertheless, several limitations should be considered. First, although age-matched [^{18}F]-FDG PET z-score mapping may improve visualization of abnormal cerebral glucose metabolism, it would not independently define the epileptogenic zone. In some cases, localization of the primary epileptogenic abnormality remains challenging, particularly those with scattered or multifocal negative z-score abnormalities, as illustrated in Figure S6. Accordingly, z-score maps should be interpreted in conjunction with structural MRI, EEG, seizure semiology, and other presurgical evaluation data. Second, the clinical case series was limited in size. The 14 pediatric epilepsy cases were included to demonstrate the feasibility and potential clinical utility of the proposed framework, but larger studies are required to determine diagnostic performance, assess reader agreement, and evaluate the added value of age-matched z-score mapping in presurgical decision-making. The results from this brain PET database from whole-body field of view successfully detected abnormalities when applied dedicated brain PET scans using different scanners; however, this was only evaluated at a single institution. The generalizability of this database and method to scans obtained at different sites was not evaluated in this study.

Summary

This study established a large-scale normative pediatric brain [^{18}F]-FDG PET database spanning ages 0–19 years and developed an age-matched z-score mapping framework for quantitative assessment of pediatric epilepsy. Voxel-wise analyses demonstrated substantial age-dependent differences in SUVR patterns across childhood and adolescence, particularly between infancy and older age groups. Whole-brain atlas normalization showed lower variability than brainstem normalization and was therefore selected for patient-level z-score mapping. Using this age-specific reference framework, z-score maps successfully identified focal or regional hypometabolism in representative pediatric epilepsy cases, including focal cortical dysplasia, malformations of cortical development, mesial temporal sclerosis, non-lesional MRI cases, remote insult, tumor-related abnormalities, and Sturge-Weber syndrome. These findings support the feasibility of using an age-matched normative pediatric [^{18}F]-FDG PET database as a quantitative adjunct to visual interpretation and multimodal presurgical evaluation.

Declarations

Acknowledgements

Conflict of Interest Statement

Seokbeen Lim, Paul H. Min, Nur Dizdar, Miguel D. Diaz, Julie B. Guerin, Michelle Silvera, Lily C. Wong-Kisiel, Hojjat Salehinejad, Gokce Belge Bilgin, Cem Bilgin, Benjamin H. Brinkmann, Jeffrey W. Britton, Derek R. Johnson, Steven Messina, Bradley J. Kemp, A. Tuba Kendi, Jun Zhang, and Val J. Lowe report no conflicts of interest relevant to this manuscript. Brian J. Burkett has consulted for Clario/Thermo Fischer Scientific, received grant support from the Americal Society of Pediatric Neuroradiology/Guerbet, and received an honorarium from Elsevier.

Author contributions

S.L. and B.J.B. conceived and designed the study, with contributions from P.H.M., L.C.W.-K., B.H.B., J.W.B., D.R.J., B.J.K., A.T.K., J.Z., and V.J.L. S.L., P.H.M., H.S., G.B.B., C.B., and B.J.B. developed and implemented the image-processing, quantitative analysis, and age-matched z-score mapping methodology. Pediatric PET/MRI data collection, image curation, and clinical imaging review were performed by S.L., N.D., M.D.D., J.B.G., M.S., D.R.J., S.M., B.J.K., A.T.K., V.J.L., and B.J.B. L.C.W.-K., B.H.B., J.W.B., and J.Z. contributed to pediatric epilepsy case characterization and clinical interpretation, with imaging interpretation support from D.R.J., S.M., B.J.K., A.T.K., V.J.L., and B.J.B. H.S. provided statistical and quantitative analysis support. S.L., P.H.M., H.S., G.B.B., and C.B. performed data processing, voxel-wise analyses, and z-score map generation. S.L. prepared the figures and visualizations, with input from P.H.M., H.S., G.B.B., C.B., B.J.K., and B.J.B. S.L. wrote the original draft of the manuscript. P.H.M., B.J.K., V.J.L., and B.J.B. supervised the study and contributed to manuscript development. All authors reviewed and edited the manuscript and approved the final version.

Funding Sources

The American Society of Pediatric Neuroradiology/Guerbet 2025 Research Grant Award supported this work.

Consent Statement

Not applicable for this retrospective study.

References

1. R. N. Menon and J. Helen Cross, "Childhood epilepsy," *The Lancet,* vol. 406, no. 10503, pp. 636-649, 2025, doi: 10.1016/S0140-6736(25)00773-1.
2. J. M. Wilmshurst, A. T. Berg, L. Lagae, C. R. Newton, and J. H. Cross, "The challenges and innovations for therapy in children with epilepsy," *Nature Reviews Neurology,* vol. 10, no. 5, pp. 249-260, 2014/05/01 2014, doi: 10.1038/nrneurol.2014.58.
3. K. C. Nickels, M. J. Zaccariello, L. D. Hamiwka, and E. C. Wirrell, "Cognitive and neurodevelopmental comorbidities in paediatric epilepsy," *Nature Reviews Neurology,* vol. 12, no. 8, pp. 465-476, 2016/08/01 2016, doi: 10.1038/nrneurol.2016.98.
4. C. Reilly *et al.*, "Neurobehavioral Comorbidities in Children With Active Epilepsy: A Population-Based Study," *Pediatrics,* vol. 133, no. 6, pp. e1586-e1593, 2014, doi: 10.1542/peds.2013-3787.
5. D. Hu *et al.*, "[18F]FDG PET for mapping the cerebral glucose metabolic characteristics of drug-sensitive and drug-resistant epilepsy in pediatric patients," *European Journal of Nuclear Medicine and Molecular Imaging,* vol. 52, no. 2, pp. 564-573, 2025/01/01 2025, doi: 10.1007/s00259-024-06933-1.
6. L. Stanescu, G. E. Ishak, P. C. Khanna, D. R. Biyyam, D. W. Shaw, and M. T. Parisi, "FDG PET of the Brain in Pediatric Patients: Imaging Spectrum with MR Imaging Correlation," *RadioGraphics,* vol. 33, no. 5, pp. 1279-1303, 2013/09/01 2013, doi: 10.1148/rg.335125152.
7. H. Jonsson *et al.*, "Epilepsies with onset during the first year of life: A prospective study on syndromes, etiologies, and outcomes," (in eng), *Epilepsia Open,* vol. 9, no. 4, pp. 1393-1405, Aug 2024, doi: 10.1002/epi4.12966.
8. C. Pedersen, M. Aboian, S. A. Messina, H. Daldrup-Link, and A. M. Franceschi, "PET/MRI Applications in Pediatric Epilepsy," (in eng), *World J Nucl Med,* vol. 22, no. 2, pp. 78-86, Jun 2023, doi: 10.1055/s-0043-1764303.
9. M. Tian *et al.*, "International consensus on the use of [18F]-FDG PET/CT in pediatric patients affected by epilepsy," *European Journal of Nuclear Medicine and Molecular Imaging,* vol. 48, no. 12, pp. 3827-3834, 2021/11/01 2021, doi: 10.1007/s00259-021-05524-8.
10. S. Minoshima, D. Cross, T. Thientunyakit, N. L. Foster, and A. Drzezga, "¹⁸F-FDG PET Imaging in Neurodegenerative Dementing Disorders: Insights into Subtype Classification, Emerging Disease Categories, and Mixed Dementia with Copathologies," *Journal of Nuclear Medicine,* vol. 63, no. Supplement 1, p. 2S, 2022, doi: 10.2967/jnumed.121.263194.

11. M. R. Ponisio *et al.*, "The Role of SPECT and PET in Epilepsy," *American Journal of Roentgenology,* vol. 216, no. 3, pp. 759-768, 2021/03/01 2021, doi: 10.2214/AJR.20.23336.
12. A. Kumar, C. Juhász, E. Asano, S. Sood, O. Muzik, and H. T. Chugani, "Objective Detection of Epileptic Foci by ¹⁸F-FDG PET in Children Undergoing Epilepsy Surgery," *Journal of Nuclear Medicine,* vol. 51, no. 12, p. 1901, 2010, doi: 10.2967/jnumed.110.075390.
13. W. D. Gaillard *et al.*, "FDG-PET in children and adolescents with partial seizures: Role in epilepsy surgery,evaluation," *Epilepsy Research,* vol. 20, no. 1, pp. 77-84, 1995/01/01/ 1995, doi: https://doi.org/10.1016/0920-1211(94)00065-5.
14. Y. Zhu *et al.*, "Glucose Metabolic Profile by Visual Assessment Combined with Statistical Parametric Mapping Analysis in Pediatric Patients with Epilepsy," *Journal of Nuclear Medicine,* vol. 58, no. 8, p. 1293, 2017, doi: 10.2967/jnumed.116.187492.
15. S. Li *et al.*, "Evaluating the Efficacy of CortexID Quantitative Analysis in Localization of the Epileptogenic Zone in Patients with Temporal Lobe Epilepsy," *Neurology and Therapy,* vol. 13, no. 5, pp. 1403-1414, 2024/10/01 2024, doi: 10.1007/s40120-024-00646-1.
16. H. T. Chugani, "A critical period of brain development: studies of cerebral glucose utilization with PET," (in eng), *Prev Med,* vol. 27, no. 2, pp. 184-8, Mar-Apr 1998, doi: 10.1006/pmed.1998.0274.
17. T. Zhang *et al.*, "High-resolution pediatric age-specific (18)F-FDG PET template: a pilot study in epileptogenic focus localization," (in eng), *Eur J Nucl Med Mol Imaging,* vol. 49, no. 5, pp. 1560-1573, Apr 2022, doi: 10.1007/s00259-021-05611-w.
18. Z. Tong, J. Wang, R. Wu, and Y. Fan, "<strong>Quantitative Localization of Epileptogenic Zones in Pediatric Epilepsy Using 18F-FDG PET/CT: Combining Z-Score and Asymmetry Index</strong&gt," *Journal of Nuclear Medicine,* vol. 66, no. supplement 1, p. 251514, 2025. [Online]. Available: http://jnm.snmjournals.org/content/66/supplement_1/251514.abstract.
19. Á. Cruz-Cortes *et al.*, "Semiquantitative analysis of cerebral [18F]FDG-PET uptake in pediatric patients," *Pediatric Radiology,* vol. 53, no. 13, pp. 2574-2585, 2023/12/01 2023, doi: 10.1007/s00247-023-05794-4.
20. R. W. Cox, "AFNI: software for analysis and visualization of functional magnetic resonance neuroimages," (in eng), *Comput Biomed Res,* vol. 29, no. 3, pp. 162-73, Jun 1996, doi: 10.1006/cbmr.1996.0014.
21. R. W. Cox and J. S. Hyde, "Software tools for analysis and visualization of fMRI data," (in eng), *NMR Biomed,* vol. 10, no. 4-5, pp. 171-8, Jun-Aug 1997, doi: 10.1002/(sici)1099-1492(199706/08)10:4/5<171::aid-nbm453>3.0.co;2-l.
22. S. Darkner. *FDG-PET template MNI152 1mm*.
23. V. S. Fonov, A. C. Evans, R. C. McKinstry, C. R. Almli, and D. L. Collins, "Unbiased nonlinear average age-appropriate brain templates from birth to adulthood," *Neuroimage,* vol. 47, p. S102, 2009/07/01/ 2009, doi: https://doi.org/10.1016/S1053-8119(09)70884-5.
24. D. L. Collins, A. P. Zijdenbos, W. F. C. Baaré, and A. C. Evans, "ANIMAL+INSECT: Improved Cortical Structure Segmentation," in *Information Processing in Medical Imaging*, Berlin, Heidelberg, A. Kuba,

M. Šáamal, and A. Todd-Pokropek, Eds., 1999// 1999: Springer Berlin Heidelberg, pp. 210-223.

25. H. T. Chugani, "Imaging Brain Metabolism in the Newborn," *Journal of Child Neurology,* vol. 33, no. 13, pp. 851-860, 2018/11/01 2018, doi: 10.1177/0883073818792308.

Tables

Tables are available in the Supplementary Files section.

Figures



Figure 1

Voxel-wise group comparison of age-related SUVR differences in the normative pediatric [^{18}F]-FDG PET cohort. Voxel-wise t-test analyses were performed across five pediatric age groups: infancy (0–1 year), early childhood period (2–5 years), middle childhood/school age (6–12 years), adolescence (13–17 years), and 4 (18–19 years). Axial slices are displayed from inferior to superior in the left-to-right direction. SUVR maps were normalized to the mean uptake of the whole-brain atlas reference region.

Statistical maps were thresholded at q < 0.05 after correction for multiple comparisons. In each A – B comparison, red voxels indicate regions with significantly higher SUVR in group A than in group B (A > B), whereas blue voxels indicate regions with significantly higher SUVR in group B than in group A (A < B). Abbreviations: FDG, fluorodeoxyglucose; PET, positron emission tomography; SUVR, standardized uptake value ratio.

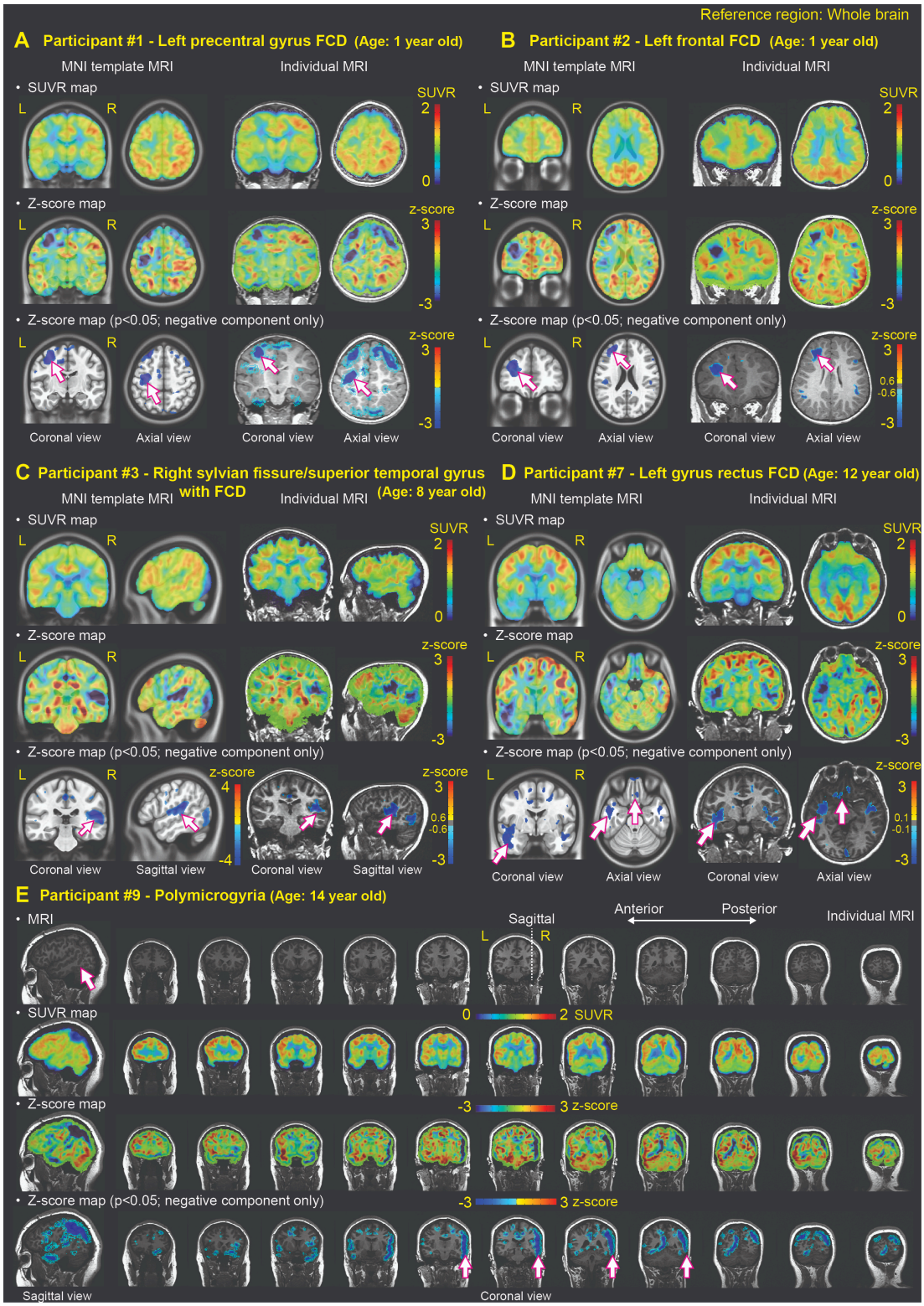


Figure 2

Age-matched z-score analysis of malformations of cortical development and focal cortical dysplasia using the normative pediatric [^{18}F]-FDG PET database. Z-score maps were generated for five representative pediatric epilepsy patients using age-specific mean and standard deviation maps derived from the normative pediatric [^{18}F]-FDG PET database. Participants 1 and 2, both 1 year old at PET imaging, were analyzed using the infancy reference group. Participants 3 and 7 were analyzed using the middle childhood/school-age reference group, and Participant 9 was analyzed using the adolescence reference group. The clinical diagnosis or imaging impression for each patient is shown next to each panel and summarized in Table 2. In panels A–D, SUVR and z-score maps are displayed in both MNI template MRI space and individual MRI space. In panel E, the individual-space MRI, SUVR map, and z-score map are shown. Z-score maps were thresholded to display only negative z-score clusters corresponding to $p < 0.05$, using a cutoff of 1.96. Arrows indicate the principal lesion or abnormal metabolic region in each patient. SUVR maps were normalized to the mean uptake of the whole-brain atlas reference region. Abbreviations: FCD, focal cortical dysplasia; FDG, fluorodeoxyglucose; MNI, Montreal Neurological Institute; MRI, magnetic resonance imaging; PET, positron emission tomography; SUVR, standardized uptake value ratio.

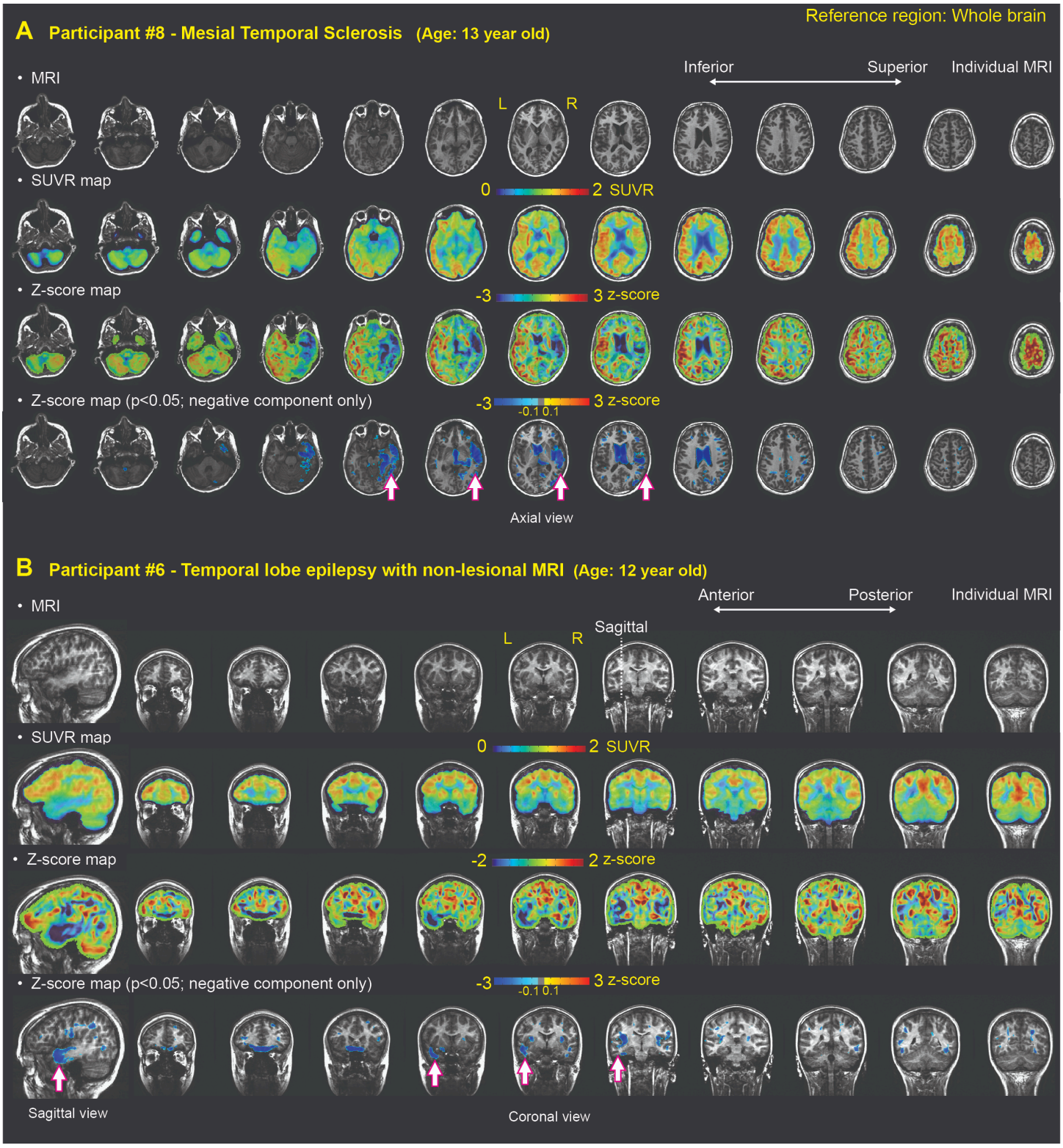


Figure 3

Age-matched z-score analysis of temporal lobe epilepsy and mesial temporal sclerosis cases using the normative pediatric [^{18}F]-FDG PET database. Z-score maps were generated for two representative pediatric epilepsy patients using age-specific mean and standard deviation maps derived from the normative pediatric [^{18}F]-FDG PET database. Participant 6, who was 12 years old at PET imaging, was analyzed using the middle childhood/school-age reference group. Participant 8, who was 13 years old at

PET imaging, was analyzed using the adolescence reference group. The clinical diagnosis or imaging impression for each patient is shown next to each panel and summarized in Table 2. In panels A and B, the individual-space MRI, SUVR map, and z-score map are displayed. Z-score maps were thresholded to show only negative z-score clusters corresponding to $p < 0.05$, using a cutoff of 1.96. Arrows indicate the principal lesion or abnormal metabolic region in each patient. SUVR maps were normalized to the mean uptake of the whole-brain atlas reference region. Abbreviations: FDG, fluorodeoxyglucose; MRI, magnetic resonance imaging; PET, positron emission tomography; SUVR, standardized uptake value ratio.

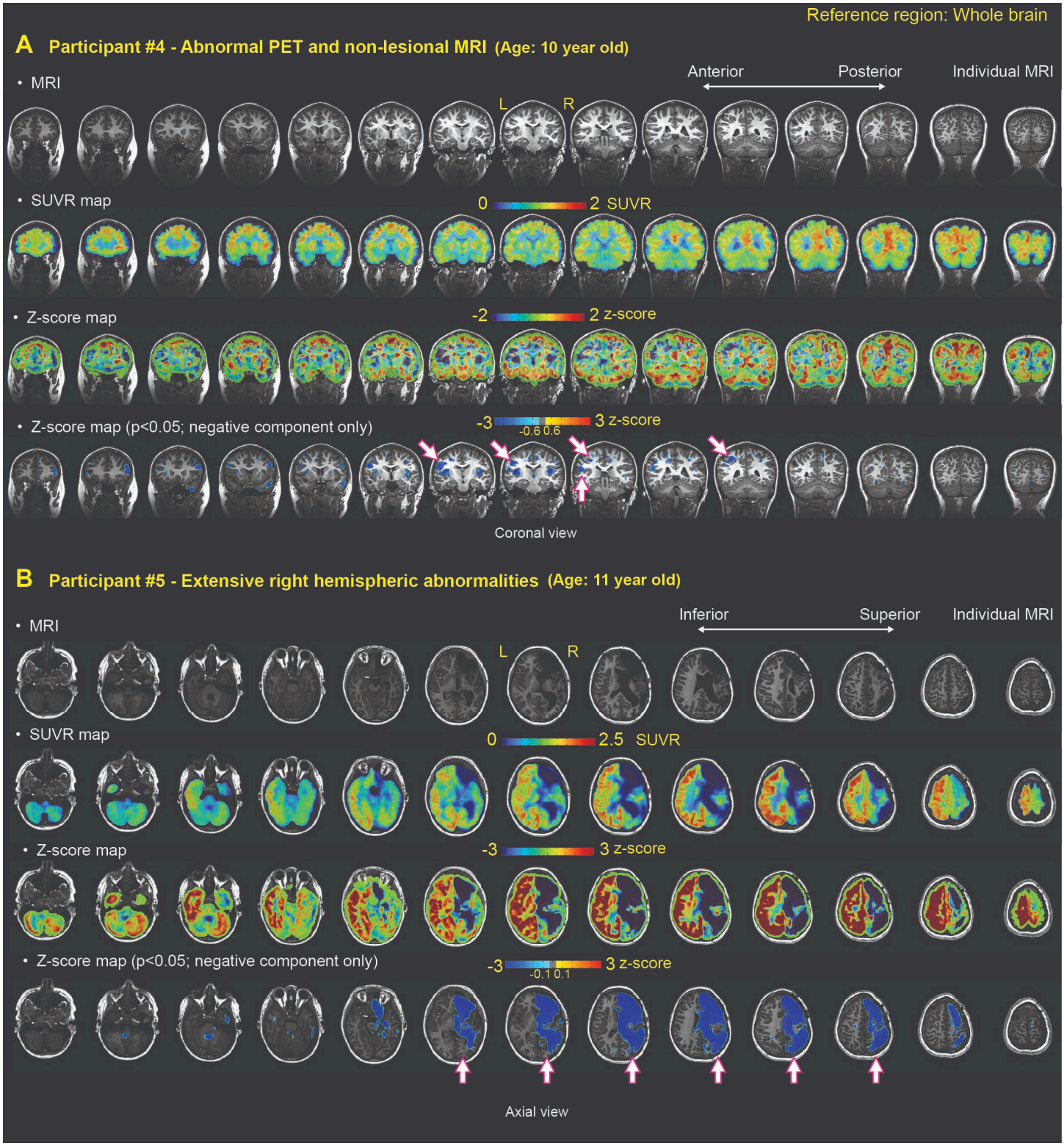


Figure 4

Age-matched z-score analysis of pediatric epilepsy cases with non-lesional MRI or extensive abnormal FDG PET findings and epilepsy associated with remote insult using the normative pediatric [^{18}F]-FDG PET database. Age-matched z-score maps were generated for two representative pediatric epilepsy patients using age-specific mean and standard deviation maps derived from the normative pediatric [^{18}F]-FDG PET database. Participant 4, who was 10 years old at the time of PET imaging, and Participant 5, who was 11 years old at the time of PET imaging, were both analyzed using the middle childhood/school-age reference group. The clinical diagnosis or imaging impression for each patient is shown next to each panel and summarized in Table 2. In panels A and B, individual-space MRI, SUVR maps, and z-score maps are displayed. Z-score maps were thresholded using a cutoff of 1.96, corresponding to $p < 0.05$, to display negative abnormalities only. Arrows indicate the principal lesion or abnormal metabolic region in each patient. SUVR maps were normalized to the mean uptake of the whole-brain atlas reference region. Abbreviations: FDG, fluorodeoxyglucose; MRI, magnetic resonance imaging; PET, positron emission tomography; SUVR, standardized uptake value ratio.

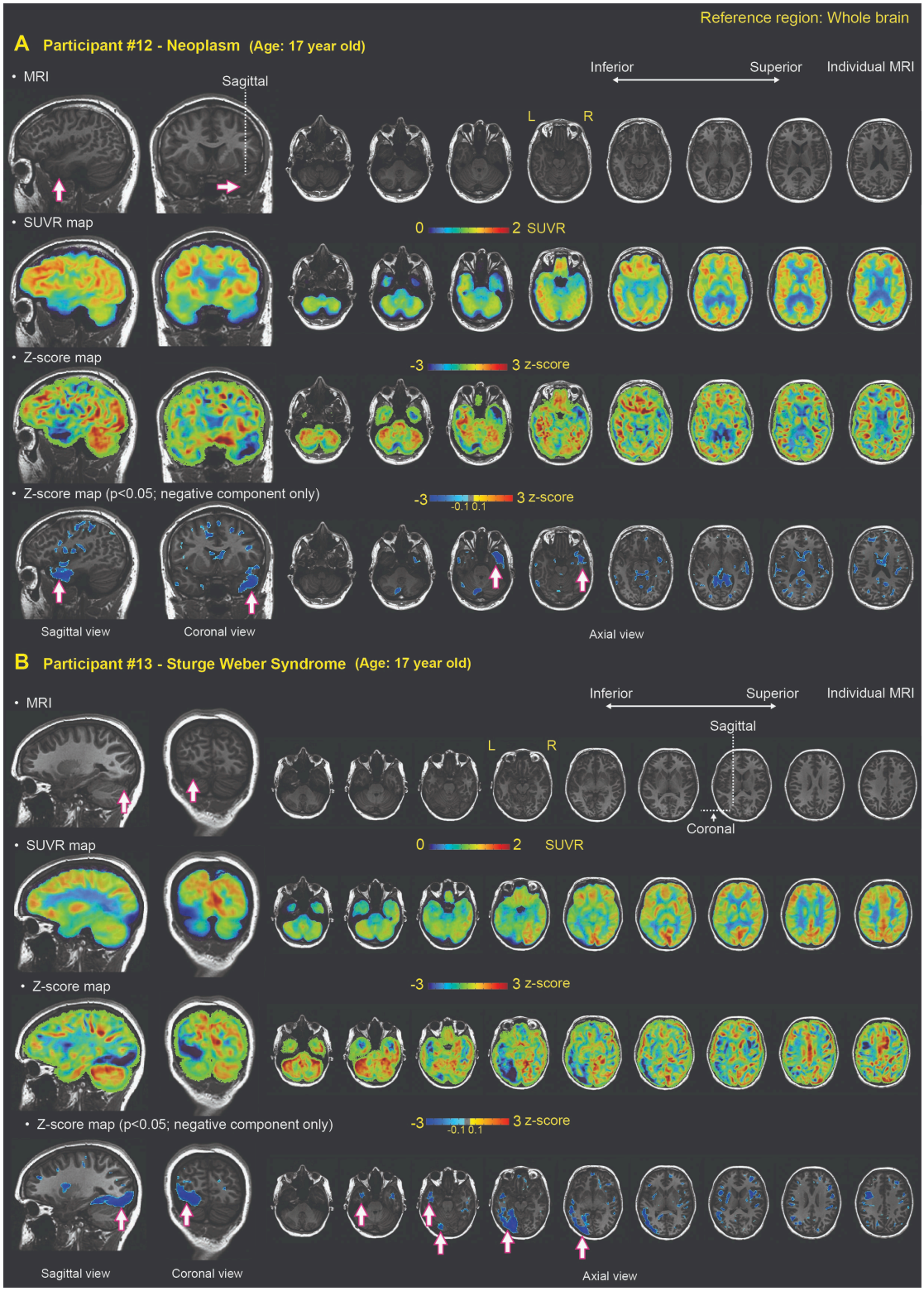


Figure 5

Age-matched z-score analysis of complex syndromic and tumor-related pediatric epilepsy cases using the normative pediatric [^{18}F]-FDG PET database. Age-matched z-score maps were generated for two representative pediatric epilepsy patients with complex syndromic or tumor-related findings using age-specific mean and standard deviation maps derived from the normative pediatric [^{18}F]-FDG PET database. Participants 12 and 13 were both 17 years old at the time of PET imaging and were analyzed

using the adolescence reference group. The clinical diagnosis or imaging impression for each patient is shown next to each panel and summarized in Table 2. In panels A and B, individual-space MRI, SUVR maps, and z-score maps are displayed. Z-score maps were thresholded using a cutoff of 1.96, corresponding to $p < 0.05$, to display negative abnormalities only. Arrows indicate the principal lesion or abnormal metabolic region in each patient. SUVR maps were normalized to the mean uptake of the whole-brain atlas reference region. Abbreviations: FDG, fluorodeoxyglucose; MRI, magnetic resonance imaging; PET, positron emission tomography; SUVR, standardized uptake value ratio.

Supplementary Files

This is a list of supplementary files associated with this preprint. Click to download.

- Table1.pdf
- Table2.pdf
- FigureS1.jpg
- FigureS2.jpg
- FigureS3.jpg
- FigureS4.jpg
- FigureS5.jpg
- FigureS6.jpg
- FigureS7.jpg